Nonlinear time-domain spectroscopy near a band inversion

Zachariah Addison and E. J. Mele
Department of Physics and Astronomy, University of Pennsylvania, Philadelphia, Pennsylvania 19104, USA

(Received 12 May 2020; accepted 31 August 2020; published 30 September 2020)

We develop a theory for the nonlinear time-domain response of a semimetal driven by an ultrafast optical pulse. At quadratic order in the driving field we find that the response near a band inversion transition contains a coherent oscillating component proportional to field intensity with a frequency that can be tuned over a wide range (from terahertz to the near IR) selected by the chemical potential. We illustrate the effect by calculating the induced current as a function of time for a two-band system with time-reversal symmetry but broken parity symmetry to study semimetals where large Berry curvature near a band inversion transition promotes this nonlinear response.

DOI: 10.1103/PhysRevB.102.115206

I. INTRODUCTION

Electrodynamic constitutive relations in the bulk of a crystal can be used to interrogate the quantum geometric character of its band structure. When formulated in the frequency domain, nonlinear responses quadratic in the driving fields have been identified as probes of the distribution of momentum space Berry curvature in systems with broken inversion symmetry [1–3] or broken mirror symmetries [4,5]. Generally, point nodes in a band structure are associated with regions of **k** space with enhanced Berry curvatures and large interband matrix elements, both of which are known to promote nonlinearities in the frequency-dependent optical response.

In many band-inverted systems large Berry curvatures are often found in the momentum space region close to a band contact point and below a small Lifshitz energy scale. Above this energy, isoenergy surfaces in the band structure do not close around isolated singularities, which prevents direct identification of the band topology. Frequency-domain spectroscopy below this Lifshitz scale typically requires interrogation at infrared or terahertz (THz) frequencies. In this work we consider instead the manifestations in nonlinear time-domain spectroscopy. We find that excitation with an ultrafast high-intensity pulse produces a nonlinear response, one part of which describes a coherent oscillation of the induced currents at a tunable frequency set by the chemical potential. We demonstrate that a nonlinear response near a Pauli blocked threshold selects a frequency-tunable response from a broadband source. This generically occurs for a narrow-gap system near a band inversion transition, and the strength of the nonlinearity can be enhanced by the large matrix elements that can be associated with a topological transition in the band structure.

This application is a variant of a class of well-studied phenomena at higher frequencies where one drives electronic motion with ultrafast high-intensity electromagnetic pulses. This family of novel nonlinear responses has been studied in interference measurements with attosecond electric fields [6–9] and has been observed in the petahertz dynamics in semiconductors like gallium nitride using few-cycle near-infrared electromagnetic pulses [10]. Similarly, in silicon the transfer of electrons from valence band states to conduction band states has been observed in the extreme-ultraviolet absorption spectrum using attosecond interferometry [11]. Subcycle motion of electrons in driven terahertz phase-locked pulses has been studied in real time by studying the interband quantum interference of electrons in Bloch states far below the Fermi energy [12,13].

Here we develop the theory for time-domain dynamics for electrons in semimetals and narrow-gap semiconductors near a band inversion transition. We study nonlinearities to quadratic order in the driving fields and show that dipole-mediated transitions between states on the Fermi surface and above the Fermi surface can generate a coherent current oscillation with a frequency tuned by the chemical potential. We find that all other allowed electronic transitions add incoherently and lead to nonoscillatory current generation. The frequency of current generated by the ultrafast pulses is set by the energy scale between the Fermi energy and the energy of the band states above the Fermi surface.

Charge currents in materials produced by nonlinear coupling to optical fields are often studied in the frequency domain [14–16]. These theoretical treatments are useful when investigating the low-frequency charge currents that are produced by the nonlinear downconversion of optical fields. For example, at second order in a perturbing electric field, DC currents like the shift and injection currents are generated by electric fields with a single frequency [17–22]. Conversely, processes like second-harmonic generation produce currents with double the frequency of the driving electric field [1–3].

Here we are interested in currents generated by ultrafast electric field pulses. The simple processes that lead to shift, injection, and second harmonic currents are difficult to isolate in this limit. Instead, we directly study the currents in a time-domain formulation and isolate second-order processes by their dependence on the field intensity. Previous work studying nonlinear responses in the time domain has focused

on two-photon photoemission and second-harmonic generation primarily for pump-probe-type measurements [23]. Here we focus on ultrashort light illumination and work in *length* gauge to extract terms that contribute to the current proportional to dipole-mediated transitions along the Fermi surface. We compute the time-dependent quantum density matrix to second order in a perturbing electric field and trace with the current operator to obtain the time-dependent induced current density. We illustrate the phenomena using a simple model for a time-reversal-symmetric, but inversion-breaking, two-dimensional semiconductor to calculate these induced currents. We find oscillating currents at frequencies selected by a Pauli threshold set by the electronic doping level of the semiconductor.

II. QUANTUM KINETIC EQUATION FOR BLOCH ELECTRONS IN AN EXTERNAL ELECTRIC FIELD

In order to calculate the time-dependent charge current to quadratic order in a perturbing electromagnetic field we first solve for the electronic charge density to second order in an external electric field by iteratively solving the quantum kinetic equation for the density matrix $\hat{\rho}(t)$. This equation derives from the von Neumann equation that describes the time evolution of this quantum operator [24]:

$$\frac{d\hat{\rho}(t)}{dt} = -\frac{i}{\hbar}[\hat{H}(t), \hat{\rho}(t)]. \tag{1}$$

The Hamiltonian can be broken into three parts, $\hat{H}(t) = \hat{H}_0 + \hat{H}' + \hat{H}_{\text{ext}}(t)$. Before application of a perturbing electromagnetic field the noninteracting part of the unperturbed Hamiltonian $\hat{H}_0$ has eigenstates $|\Psi_n(\boldsymbol{k})\rangle$ that are crystalline Bloch modes whose energy $\varepsilon_n(\boldsymbol{k})$ is indexed by the state's crystal momentum $\boldsymbol{k}$ and band n and whose periodic part we denote by the ket $|u_n(\boldsymbol{k})\rangle$. We can write the von Neumann equation in this unperturbed basis and denote matrix elements of the density matrix as $\rho_{nm}(\boldsymbol{k}, t) = \langle\Psi_n(\boldsymbol{k})|\,\hat{\rho}(t)\,|\Psi_m(\boldsymbol{k})\rangle$. We will consider spatially homogeneous perturbing fields $\boldsymbol{E}(\boldsymbol{r}, t) \to \boldsymbol{E}(t)$ that couple only Bloch electrons with the same Bloch wave vector $\boldsymbol{k}$ such that the perturbed density matrix is diagonal in crystal momentum $\boldsymbol{k}$: $\langle\Psi_n(\boldsymbol{k})|\,\hat{\rho}(t)\,|\Psi_m(\boldsymbol{k}')\rangle = \delta_{\boldsymbol{k},\boldsymbol{k}'}\langle\Psi_n(\boldsymbol{k})|\,\hat{\rho}(t)\,|\Psi_m(\boldsymbol{k})\rangle$. Here we treat the coupling of the electromagnetic field to fermionic matter in the electronic dipole approximation $\hat{H}_{\text{ext}}(t) = e\boldsymbol{E}(t)\cdot\hat{\boldsymbol{r}}$ [25]. The von Neumann equation can then be written as

$$\frac{d\hat{\rho}(t)}{dt} = -\frac{i}{\hbar}[\hat{H}_0(t), \hat{\rho}(t)] - \frac{i}{\hbar}[e\hat{\boldsymbol{r}}\cdot\boldsymbol{E}(t), \hat{\rho}(t)] - \frac{i}{\hbar}[\hat{H}', \hat{\rho}(t)]. \tag{2}$$

For simplicity we encode the effects of other interactions in our system in a relaxation time approximation such that $-i/\hbar[\hat{H}', \rho(t)] \approx -[\hat{\rho}(t) - \hat{\rho}_0]/\tau$, where $\hat{\rho}_0$ is the unperturbed density matrix. In the Bloch basis we have $\langle\Psi_n(\boldsymbol{k})|\,\hat{H}_0\,|\Psi_m(\boldsymbol{k})\rangle = \delta_{nm}\varepsilon_n(\boldsymbol{k})$ and $\langle\Psi_n(\boldsymbol{k})|\,\hat{\boldsymbol{r}}\,|\Psi_m(\boldsymbol{k})\rangle = \langle u_n(\boldsymbol{k})|\,i\partial_{\boldsymbol{k}}\,|u_m(\boldsymbol{k})\rangle$ [26]. Substitution into Eq. (2) leads to the quantum kinetic equation for the density matrix written in the Bloch basis and perturbed by a time-dependent homogeneous external electric field [27]:

$$\frac{\partial\rho_{nm}(\boldsymbol{k}, t)}{\partial t} + \left(\frac{i}{\hbar}[\varepsilon_n(\boldsymbol{k}) - \varepsilon_m(\boldsymbol{k})] + \frac{1}{\tau}\right)\rho_{nm}(\boldsymbol{k}, t) - \frac{\delta_{nm}f_n^T(\boldsymbol{k}, \mu)}{\tau} = \sum_{i,l}\frac{eE_i(t)}{\hbar}\big(\partial_{k_i}\rho_{nm}(\boldsymbol{k}, t) - i\big[R^i_{nl}(\boldsymbol{k})\rho_{lm}(\boldsymbol{k}, t) - \rho_{nl}(\boldsymbol{k}, t)R^i_{lm}(\boldsymbol{k})\big]\big). \tag{3}$$

Here $f_n^T(\boldsymbol{k}, \mu)$ is the Fermi occupation function that depends on both the temperature T and chemical potential μ of the system, $R^i_{nm}(\boldsymbol{k}) = \langle u_n(\boldsymbol{k})|\,i\partial_{k_i}\,|u_m(\boldsymbol{k})\rangle$ are the matrix elements of the dipole operator, and τ is a phenomenological relaxation constant arising from the relaxation time approximation denoted above. As will be shown, this constant will set the timescale for the system to return to its unperturbed equilibrium configuration.

Gauge covariance

The dynamics of the system, like the charge density and current density, should be invariant under gauge transformations of the Bloch functions of the form $|\Psi_n(\boldsymbol{k})\rangle \to e^{i\theta_n(\boldsymbol{k})}|\Psi_n(\boldsymbol{k})\rangle$ for all n. As such the quantum kinetic equation for the quantum density matrix should remain covariant under such a transformation. The matrix elements of both the density operator $\rho_{nm}(\boldsymbol{k}, t)$ and dipole operator $\boldsymbol{R}_{nm}(\boldsymbol{k})$ are changed by the gauge transformations $|\Psi_n(\boldsymbol{k})\rangle \to e^{i\theta_n(\boldsymbol{k})}|\Psi_n(\boldsymbol{k})\rangle$ via

$$\rho_{nm}(\boldsymbol{k}, t) \to e^{i(\theta_m(\boldsymbol{k})-\theta_n(\boldsymbol{k}))}\rho_{nm}(\boldsymbol{k}, t), \tag{4}$$

$$\boldsymbol{R}_{nm}(\boldsymbol{k}) \to e^{i(\theta_m(\boldsymbol{k})-\theta_n(\boldsymbol{k}))}\boldsymbol{R}_{nm}(\boldsymbol{k}) + \delta_{nm}i\nabla\theta_m(\boldsymbol{k}). \tag{5}$$

The left-hand side of Eq. (3) under this gauge transformation is simply multiplied by the phase $e^{i[\theta_m(\boldsymbol{k})-\theta_n(\boldsymbol{k})]}$, while elements on the right-hand side of Eq. (3) transform as

$$\partial_{k_i}\rho_{nm}(\boldsymbol{k}, t) \to e^{i[\theta_m(\boldsymbol{k})-\theta_n(\boldsymbol{k})]}(\partial_{k_i}\rho_{nm}(\boldsymbol{k}, t) + i\rho_{nm}(\boldsymbol{k}, t)[\partial_{k_i}\theta_m(\boldsymbol{k}) - \partial_{k_i}\theta_n(\boldsymbol{k})]), \tag{6}$$

$$\sum_l R^i_{nl}(\boldsymbol{k})\rho_{lm}(\boldsymbol{k}, t) \to e^{i[\theta_m(\boldsymbol{k})-\theta_n(\boldsymbol{k})]}\left(\sum_l R^i_{nl}(\boldsymbol{k})\rho_{lm}(\boldsymbol{k}, t) - i\partial_i\theta_n(\boldsymbol{k})\rho_{nm}(\boldsymbol{k}, t)\right). \tag{7}$$

Combining the above results demonstrates that the right-hand side of Eq. (3) is also simply multiplied by the phase $e^{i[\theta_m(\boldsymbol{k})-\theta_n(\boldsymbol{k})]}$ under this type of gauge transformation, implying that the quantum kinetic equation for the density matrix is gauge covariant. The solutions to the quantum kinetic equation for the density matrix $\rho_{nm}(\boldsymbol{k}, t)$ will maintain this covariance such that the density $\text{Tr}[\hat{\rho}(t)]$ and the current density $\text{Tr}[\hat{\rho}(t)e\hat{\boldsymbol{v}}]$ are invariant under these gauge transformations.

III. CURRENT DENSITIES FIRST ORDER IN AN EXTERNAL ELECTRIC FIELD

Charge currents that are linearly proportional to the electric field can be found by solving Eq. (3) for the density matrix to first order in the electric field. First, we expand the density matrix in powers of the electric field $\rho_{nm}(\boldsymbol{k}) = \sum_p \rho^{(p)}_{nm}(\boldsymbol{k})$, where p indexes the order to which $\rho^{(p)}_{nm}(\boldsymbol{k})$ is proportional to $\boldsymbol{E}(t)$. For $p = 0$ the density matrix is unperturbed by the electric field, and the solution to Eq. (3) at zeroth order in the external field is just the equilibrium Fermi distribution: $\rho^{(0)}_{nm} = \delta_{nm} f^T_n(\boldsymbol{k}, \mu)$. The first-order equation can now be written as

$$\frac{\partial \rho^{(1)}_{nm}(\boldsymbol{k}, t)}{\partial t} + \alpha_{nm}(\boldsymbol{k})\rho^{(1)}_{nm}(\boldsymbol{k}, t) = \frac{e\boldsymbol{E}(t) \cdot \boldsymbol{g}_{nm}(\boldsymbol{k})}{\hbar}, \quad (8)$$

where the density matrix to first order in the electric field $\rho^{(1)}_{nm}$ couples to $\alpha_{nm}(\boldsymbol{k}) = i/\hbar[\varepsilon_n(\boldsymbol{k}) - \varepsilon_m(\boldsymbol{k})] + 1/\tau$ and the external perturbing field couples to $g^i_{nm}(\boldsymbol{k}) = \delta_{nm}\partial_i f^T_n(\boldsymbol{k}, \mu) + i[f^T_n(\boldsymbol{k}, \mu) - f^T_m(\boldsymbol{k}, \mu)]R^i_{nm}(\boldsymbol{k})$. At zero temperature this coupling leads to two types of terms in the equation of motion for the density matrix. For $T = 0$ terms proportional to $\partial_i f^T_n(\boldsymbol{k}, \mu)$ are only nonzero on the Fermi surface as $\partial_i f^{T=0}_n(\boldsymbol{k}, \mu) = \partial_{k_i}\varepsilon_n(\boldsymbol{k})\delta[\varepsilon_n(\boldsymbol{k}) - \mu]$, leading to intraband processes that contribute to $\rho_{nm}(\boldsymbol{k}, t)$. The other terms in $g^i_{nm}(\boldsymbol{k})$ describe interband processes mediated by the matrix elements of the dipole operator $\boldsymbol{R}_{nm}(\boldsymbol{k})$.

The solution to Eq. (8) is

$$\rho^{(1)}_{nm}(\boldsymbol{k}, t) = \int_{t_p}^{t} dt' e^{-\alpha_{nm}(\boldsymbol{k})(t-t')} \frac{e\boldsymbol{E}(t') \cdot \boldsymbol{g}_{nm}(\boldsymbol{k})}{\hbar}. \quad (9)$$

Here we have assumed that the perturbing electric field is zero for times $t < t_p$ [$\boldsymbol{E}(t) \sim \theta(t - t_p)$]. Equation (8) demonstrates that, indeed, $\rho^{(1)}_{nm}(\boldsymbol{k}, t)$ are matrix elements of a Hermitian operator such that taking its trace with respect to n, m, and $\boldsymbol{k}$ or the trace of a product of it and other Hermitian operators will lead to quantities whose values are purely real. The associated current density, for example, whose values are purely real is found by tracing over the operator product $e\hat{v}\hat{\rho}(t)$:

$$\boldsymbol{j}(t) = \frac{1}{V}\sum_{k,n,m} e\boldsymbol{v}_{nm}(\boldsymbol{k})\rho_{mn}(\boldsymbol{k}, t). \quad (10)$$

Here $v^i_{nm}(\boldsymbol{k})$ are the matrix elements of the velocity operator in the $\hat{\boldsymbol{i}}$ direction written in the Bloch basis. In general $\hat{\boldsymbol{v}} = i/h[\hat{H}, \hat{\boldsymbol{r}}]$. Here we work in length gauge, where the coupling of fermionic matter to the external electric field can be written as $e\boldsymbol{E}(t) \cdot \boldsymbol{r}$. For this electromagnetic gauge choice the velocity operator is $\hat{\boldsymbol{v}} = i/h[\hat{H}_0, \hat{\boldsymbol{r}}]$ and independent of the electric field. Here we choose the gauge on the Bloch states $|u_n(\boldsymbol{k})\rangle$ such that the velocity operator takes the representation

$$v^i_{nm}(\boldsymbol{k}) = \frac{1}{\hbar}\langle u_n(\boldsymbol{k})| \partial_{k_i}\hat{H}_0(\boldsymbol{k}) |u_m(\boldsymbol{k})\rangle . \quad (11)$$

If we had decided to work in the *velocity* gauge, where the coupling to the external electromagnetic potential is described by the perturbation $\hat{H}'(\boldsymbol{k}) \sim \boldsymbol{v}(\boldsymbol{k}) \cdot \boldsymbol{A}(t)$, the velocity operator would contain terms proportional to the external perturbing field [16,25]. In this work we choose to work in length gauge, where the velocity operator is independent of the perturbing electric field and is simply given by Eq. (11).

Usually, one is interested in systems perturbed by electric fields that are oscillatory in time with a single frequency ω. In these cases it is usually advantageous to look at the Fourier transform $\boldsymbol{\mathcal{J}}(\omega) = \int dt e^{-i\omega t}\boldsymbol{j}(t)$ of the current density $\boldsymbol{j}(t)$. Equation (9) is in the form of a convolution such that the Fourier transform of $\boldsymbol{j}(t)$ to first order in the electric field is simply

$$\boldsymbol{\mathcal{J}}^{(1)}(\omega) = \frac{1}{V}\sum_{k,n,m} \frac{e^2\boldsymbol{E}(\omega) \cdot \boldsymbol{g}_{nm}(\boldsymbol{k})}{\hbar\alpha_{nm} - i\hbar\omega}\boldsymbol{v}_{mn}(\boldsymbol{k}), \quad (12)$$

where, again, $\alpha_{nm}(\boldsymbol{k}) = i/\hbar(\varepsilon_n(\boldsymbol{k}) - \varepsilon_m(\boldsymbol{k})) + 1/\tau$.

Here we are interested in electric field pulses that are short compared to all other timescales of our system. We thus consider an electric field pulse $\boldsymbol{E}(t) = \boldsymbol{E}_0\Delta_t\delta(t - t_0)$. For this type of perturbing field the first-order contribution to the current is

$$\boldsymbol{j}^{(1)}(t) = \frac{\theta(t - t_0)}{V}\sum_{k,n,m} e^{-\alpha_{nm}(t-t_0)}\frac{e^2\boldsymbol{E}_0 \cdot \boldsymbol{g}_{nm}(\boldsymbol{k})}{\hbar}\Delta_t\boldsymbol{v}_{mn}(\boldsymbol{k}). \quad (13)$$

The current decays exponentially in time [$\boldsymbol{j}^{(1)}(t) \sim e^{-(t-t_0)/\tau}$]. At zero-temperature intraband contributions proportional to the diagonal part of the velocity matrix $\boldsymbol{v}_{nm}(\boldsymbol{k})$ on the Fermi surface are nonoscillatory as $\alpha_{nn}(\boldsymbol{k})$ is purely real, while interband contributions between bands n and m oscillate with frequency $[\varepsilon_n(\boldsymbol{k}) - \varepsilon_m(\boldsymbol{k})]/\hbar$. These interband contributions are summed incoherently across all crystal momentum, leading to smooth behavior of $\boldsymbol{j}^{(1)}(t)$ for all times $t > t_p$.

IV. CURRENT DENSITIES SECOND ORDER IN AN EXTERNAL ELECTRIC FIELD

The current density to second order in a perturbing electric field can be found by solving Eq. (3) for the density matrix to second order in the perturbation. Like in the previous section we first expand the density matrix in powers of the electric field and equate terms on the left- and right-hand sides of Eq. (3) that are quadratically proportional to the perturbation. This leads to a second-order equation for $\rho^{(2)}_{nm}(\boldsymbol{k}, t)$,

$$\frac{\partial \rho^{(2)}_{nm}(\boldsymbol{k}, t)}{\partial t} + \left(\frac{i}{\hbar}[\varepsilon_n(\boldsymbol{k}) - \varepsilon_m(\boldsymbol{k})] + \frac{1}{\tau}\right)\rho^{(2)}_{nm}(\boldsymbol{k}, t) = \sum_{i,l}\frac{eE_i(t)}{\hbar}\left(\partial_{k_i}\rho^{(1)}_{nm}(\boldsymbol{k}, t) - i\left[R^i_{nl}(\boldsymbol{k})\rho^{(1)}_{lm}(\boldsymbol{k}, t) - \rho^{(1)}_{nl}(\boldsymbol{k}, t)R^i_{lm}(\boldsymbol{k})\right]\right). \quad (14)$$

With knowledge of $\rho^{(1)}_{nm}(\boldsymbol{k},t)$ we can use this equation to solve for $\rho^{(2)}_{nm}(\boldsymbol{k},t)$. The solution can be broken into three parts,

$$\rho^{(2)}_{nm}(\boldsymbol{k},t)=\int_{t_p}^{t}dt''\int_{t_p}^{t''}dt'\frac{e^2}{\hbar^2}\sum_{ij}E_j(t'')E_i(t')e^{-\alpha_{nm}(\boldsymbol{k})(t-t'')}\big[\chi^1_{ij,nm}(\boldsymbol{k},t',t'')+\chi^2_{ij,nm}(\boldsymbol{k},t',t'')+\chi^3_{ij,nm}(\boldsymbol{k},t',t'')\big]. \tag{15}$$

Here the tensors $\chi^p_{ij}(\boldsymbol{k},t',t'')$ each contribute uniquely to the quantum density matrix:

$$\begin{aligned}
\chi^1_{ij,nm}(\boldsymbol{k},t',t'')&=\partial_{k_j}\alpha_{nm}(\boldsymbol{k})(t'-t'')e^{-\alpha_{nm}(t''-t')}g^i_{nm}(\boldsymbol{k}),\\
\chi^2_{ij,nm}(\boldsymbol{k},t',t'')&=e^{-\alpha_{nm}(\boldsymbol{k})(t''-t')}\partial_{k_j}g^i_{nm}(\boldsymbol{k}),\\
\chi^3_{ij,nm}(\boldsymbol{k},t',t'')&=\sum_l\left(-iR^j_{nl}(\boldsymbol{k})g^i_{lm}(\boldsymbol{k})e^{-\alpha_{lm}(\boldsymbol{k})(t''-t')}+ig^i_{nl}(\boldsymbol{k})R^j_{lm}(\boldsymbol{k})e^{-\alpha_{nl}(\boldsymbol{k})(t''-t')}\right).
\end{aligned} \tag{16}$$

To demonstrate the solution to these equations for short electric field pulses we again use $\boldsymbol{E}(t)=\boldsymbol{E}_0\Delta_t\delta(t-t_0)$. Integration in Eq. (15) over this field leads to $t'\to t_0$ and $t''\to t_0$. The first contribution to the second-order density vanishes as $\chi^1_{ij,nm}(\boldsymbol{k},t_0,t_0)=0$. This leads to the current density

$$\boldsymbol{j}^{(2)}(t)=\frac{\theta(t-t_0)}{V}\sum_{n,m,i,j}\frac{e^3}{\hbar^2}e^{-\alpha_{nm}(\boldsymbol{k})(t-t_0)}\boldsymbol{v}_{mn}(\boldsymbol{k})E^i_0E^j_0\Delta_t^2\times\left(\partial_jg^i_{nm}(\boldsymbol{k})-i\big[R^j_{nl}(\boldsymbol{k})g^i_{lm}(\boldsymbol{k})-g^i_{nl}(\boldsymbol{k})R^j_{lm}(\boldsymbol{k})\big]\right). \tag{17}$$

At zero temperature we can further divide this response into two pieces, $\boldsymbol{j}^{(2)}(t)=1/V\sum_k[\boldsymbol{j}_A(\boldsymbol{k},t)+\boldsymbol{j}_B(\boldsymbol{k},t)]$. Here $\boldsymbol{j}_A(\boldsymbol{k},t)$ is nonzero only at the crystal momentum on the Fermi surface, while $\boldsymbol{j}_B(\boldsymbol{k},t)$ has support across the entire Brillouin zone. This division can be done uniquely after demanding that each contribution be itself gauge invariant [28]. With this constraint,

$$\begin{aligned}
\boldsymbol{j}_A(\boldsymbol{k},t)=&\sum_{n,m,i,j}\frac{e^3}{V\hbar}E^i_0E^j_0\Delta_t^2\delta(\varepsilon_n-\mu)v^i_{nn}(\boldsymbol{k})\\
&\times\left\{-\delta_{nm}\partial_jv^p_{nm}(\boldsymbol{k})e^{-\alpha_{nm}(\boldsymbol{k})(t-t_0)}+2i\big[e^{-\alpha_{nm}(\boldsymbol{k})(t-t_0)}R^j_{nm}(\boldsymbol{k})v^p_{mn}(\boldsymbol{k})-e^{-\alpha_{mn}(\boldsymbol{k})(t-t_0)}v^p_{nm}(\boldsymbol{k})R^j_{mn}(\boldsymbol{k})\big]\right\},
\end{aligned} \tag{18}$$

$$\begin{aligned}
\boldsymbol{j}_B(\boldsymbol{k},t)=&\sum_{n,m,i,j}\frac{e^3}{V\hbar^2}E^i_0E^j_0\Delta_t^2e^{-\alpha_{nm}(\boldsymbol{k})(t-t_0)}\Bigg(\big[f^{T=0}_n(\boldsymbol{k},\mu)-f^{T=0}_m(\boldsymbol{k},\mu)\big]i\partial_{k_i}R^j_{nm}(\boldsymbol{k})v^p_{mn}(\boldsymbol{k})\\
&+\sum_l\big\{2f^{T=0}_l(\boldsymbol{k},\mu)-\big[f^{T=0}_n(\boldsymbol{k},\mu)+f^{T=0}_m(\boldsymbol{k},\mu)\big]\big\}R^i_{nl}(\boldsymbol{k})R^j_{lm}(\boldsymbol{k})v^p_{mn}(\boldsymbol{k})\Bigg).
\end{aligned} \tag{19}$$

Both contributions decay exponentially in time with timescale τ. Each contribution $\boldsymbol{j}_B(\boldsymbol{k},t)$ oscillates with a frequency determined by the energy differences between bands. This incoherent summation over the entire Brillouin zone leads to a contribution to the current smooth in time (see Fig. 4 below). The contributions $\boldsymbol{j}_A(\boldsymbol{k},t)$ each have two parts. One part is proportional to the diagonal elements of $\alpha_{nm}(\boldsymbol{k})$, leading to nonoscillatory contributions to the current. The other part oscillates with frequency again defined by the energy difference between bands. We will show in the next section that for certain band structures the sum of these terms across the Fermi surface can add coherently when the energy differences between band states on the Fermi surface and the states just above the Fermi surface are nearly constant. This coherent superposition of terms that oscillate at a fixed frequency can lead to currents that oscillate in time with frequency determined by these energy differences, as we will now demonstrate.

V. MINIMAL MODELS FOR OSCILLATORY CHARGE CURRENT GENERATION

In the previous section we proved that the induced charge current to second order in an ultrafast electric field pulse has two contributions. The contribution deriving from $\boldsymbol{j}_B(\boldsymbol{k},t)$ develops a contribution to the current that is smooth in time, and the contribution $\boldsymbol{j}_A(\boldsymbol{k},t)$, for the right model, can develop a contribution to the current that oscillates in time with a nearly constant frequency. Here we demonstrate this phenomenon in a minimal two-band model.

The model consists of a continuum theory of two valleys that can represent the low-energy dynamics of spinless electrons in a two-dimensional crystal. The Bloch Hamiltonian in an orbital basis takes the form

$$\hat{H}_\chi(\boldsymbol{k})=\chi\hbar\boldsymbol{b}\cdot\boldsymbol{k}\mathbb{I}+\hbar v_F(\chi k_x\sigma_x+k_y\sigma_y)+m_0\sigma_z. \tag{20}$$

Here $\chi=\pm1$ indexes the valley degree of freedom. For spinless electrons time reversal $\mathcal{T}$ is just the complex-conjugation operator $\mathcal{K}$. We imagine that the valleys are centered at opposite crystal momenta in the Brillouin zone such that the Hamiltonian is time reversal invariant and satisfies $\hat{H}^*_\chi(\boldsymbol{k})=\hat{H}_{-\chi}(-\boldsymbol{k})$. For vanishing m_0 and $\boldsymbol{b}$ the theory consists of linear bands that cross at $\boldsymbol{k}_0=(0,0)$ for each valley [Fig. 1(a)]. In this limit the Hamiltonian has a chiral symmetry $\{\hat{H}_\chi(\boldsymbol{k}),\sigma_z\}=0$ such that its energy eigenvalues come in plus-minus pairs. Also in this limit the Hamiltonian satisfies $\sigma_x\hat{H}_\chi(\boldsymbol{k})\sigma_x=\hat{H}_{-\chi}(-\boldsymbol{k})$ and has inversion symmetry. Nonzero $\boldsymbol{b}$ tilts the linear bands such that the chiral symmetry

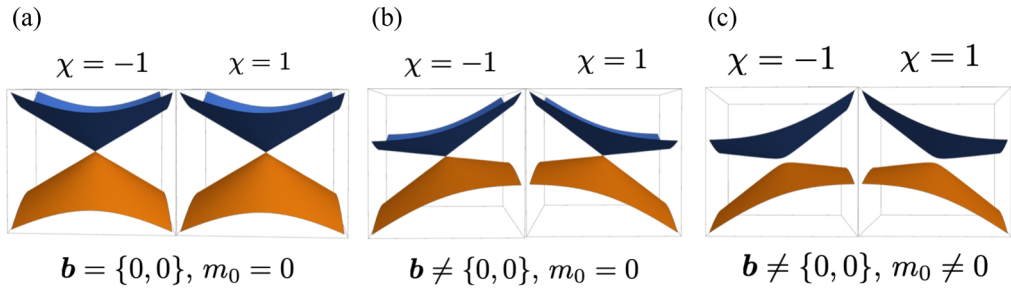

FIG. 1. (a)–(c) Band structures of various two-band models described by Eq. (20). (a) Model preserving time-reversal, inversion, and chiral symmetries. (b) Model with time-reversal and inversion symmetries but with broken chiral symmetry. (c) Model with time-reversal symmetry but broken inversion and chiral symmetries.

is broken and the spectrum at each valley no longer consists of plus-minus pairs [Fig. 1(b)]. Nonzero m_0 breaks inversion and introduces a gap that breaks the twofold-degenerate crossing at $\boldsymbol{k}_0$ for each valley [Fig. 1(c)].

For our ultrafast electric field pulses $\boldsymbol{E}(t) = \boldsymbol{E}_0 \Delta_t \delta(t - t_0)$ the intraband contribution to the current will be nonzero if both chiral and inversion symmetries are broken and at electron fillings for which the chemical potential sits below the energy gap. In these situations the Fermi surface will be an ellipse in the $k_x k_y$ plane. The contributions $\boldsymbol{j}_A(\boldsymbol{k}, t)$ come from transitions between these Fermi surface states and the states in the unoccupied band with the same Bloch momenta. These terms each have a contribution that oscillates at a frequency determined by the energy difference between these bands at momenta along the Fermi surface. For vanishing $\boldsymbol{b}$ the energy difference would be constant across the Fermi surface and equal to 2μ. This would lead to terms $\boldsymbol{j}_A(\boldsymbol{k}, t)$ that oscillate at frequency $\omega = 2\mu/\hbar$. Nonzero $\boldsymbol{b}$ leads to a distribution of energy differences across the Fermi surface. Figure 2 shows the band structure in a single valley for a typical time-reversal-invariant but chiral- and inversion-broken system. The Fermi surface is schematically shown in red. States with momenta along the Fermi surface but in the unoccupied band are shown in purple. The terms $\boldsymbol{j}_A(\boldsymbol{k}, t)$ contributing to the Fermi surface contribution to the current will oscillate over a range of frequencies: $\Delta E_{min}/\hbar \leqslant \omega \leqslant \Delta E_{max}/\hbar$, where ΔE_{max} and ΔE_{min} depend on m_0, $\boldsymbol{b}$, and μ.

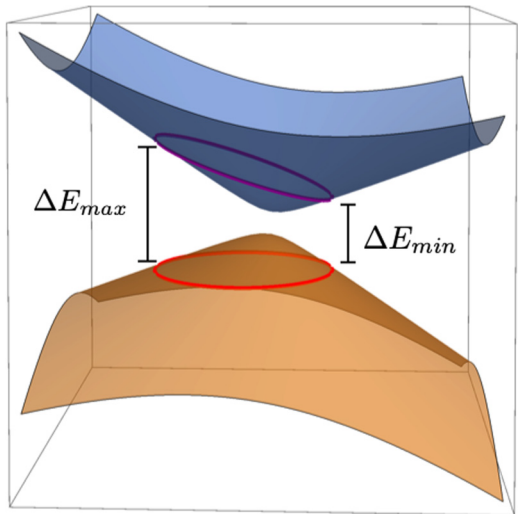

FIG. 2. Typical time-reversal-invariant, inversion, and chiral-breaking band structure for a single valley χ. The Fermi surface is schematically shown in red. Contributions to $\boldsymbol{j}^{\text{intra}}(\boldsymbol{k})$ derive from interband matrix elements between states on the Fermi surface and Bloch states along the purple ellipse. Terms in $\boldsymbol{j}^{\text{intra}}(\boldsymbol{k})$ oscillate at frequencies $\Delta E_{\text{min}}/\hbar \leqslant \omega \leqslant \Delta E_{\text{max}}/\hbar$.

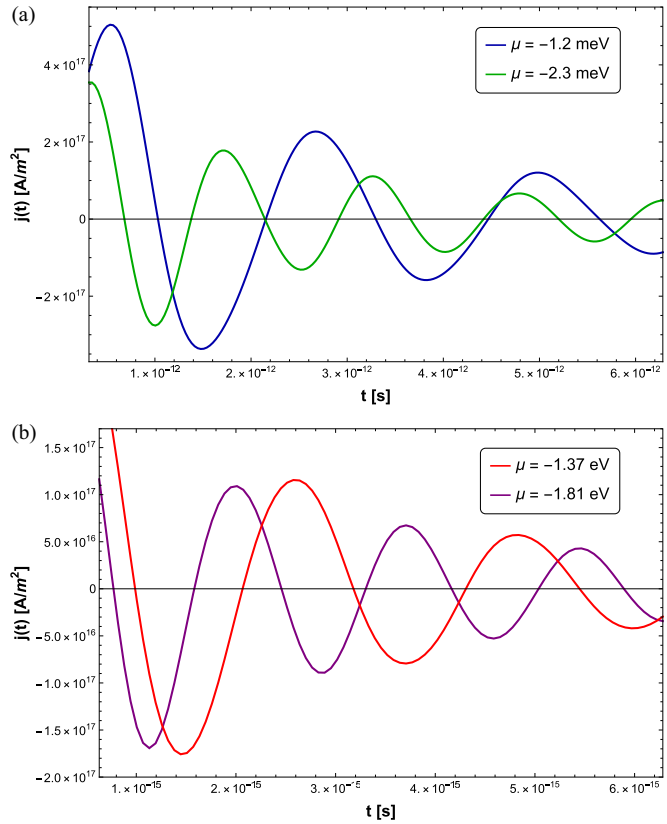

FIG. 3. The contribution to the current arising from $\boldsymbol{j}_A(\boldsymbol{k}, t)$ as a function of time for a system with $\boldsymbol{b} = (0.5, 0.2)v_f$, $v_f = 10^6$ m/s, and $\tau = 6.3 \times 10^{-15}$ s perturbed by an electric field pulse with $\Delta_t = 0.2$ ps and $E_0 = 5$ MV/cm. (a) System with small gap size $m_0 = 0.001\hbar v_f/a$ for two different chemical potentials, $\mu = -1.2$ meV and $\mu = -2.3$ meV, with average terahertz frequency modulation $\bar{\omega} = 2.79 \times 10^{12}$ s^{-1} and $\bar{\omega} = 4.21 \times 10^{12}$ s^{-1}, respectively. (b) System with large gap size $m_0 = 0.5\hbar v_f/a$ for two different chemical potentials, $\mu = -1.37$ eV and $\mu = -1.81$ eV, with average petahertz frequency modulation $\bar{\omega} = 2.86 \times 10^{15}$ s^{-1} and $\bar{\omega} = 3.69 \times 10^{15}$ s^{-1}, respectively.

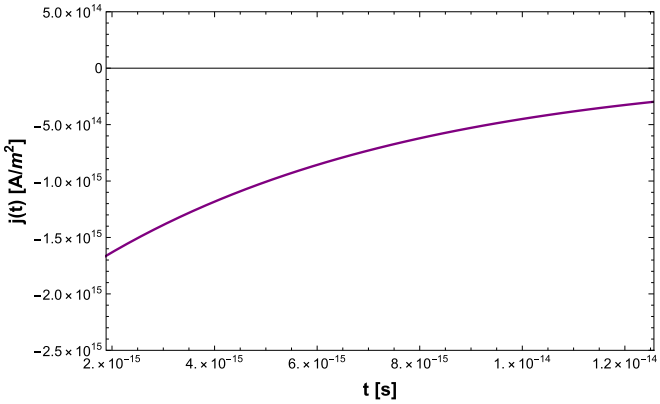

FIG. 4. Example of the contribution to the current arising from contributions $\boldsymbol{j}_B(\boldsymbol{k}, t)$ with model parameters $\boldsymbol{b} = (0.5, 0.2)v_f$, $v_f = 10^6$ m/s, $\tau = 6.3 \times 10^{-15}$, $\Delta_t = 0.2$ ps, $E_0 = 5$ MV/cm, $m_0 = 0.5\hbar v_f/a$, and $\mu = -1.37$ eV. These contributions to the currents oscillate at frequencies determined by the energy difference between bands and tend to add incoherently across the Brillouin zone, producing a nonoscillatory current that decays exponentially in time.

In order to observe an oscillatory current generated from an ultrafast electric field pulse the terms in $\boldsymbol{j}_A(\boldsymbol{k}, t)$ must add coherently, and thus, we must be in the limit where $(\Delta E_{\max} - \Delta E_{\min})/\hbar \ll \Delta\bar{E}$, where $\Delta\bar{E}$ is the average energy difference between the two bands across the Fermi surface. In this regime these interband matrix coefficients will lead to a current that oscillates with frequency $\bar{\omega} = \Delta\bar{E}/\hbar$. To tune this frequency one can adjust the chemical potential of the system, thereby changing the average energy difference between the two bands around crystal momentum along the Fermi surface and thus changing $\bar{\omega}$. Furthermore, the current generated from these ultrafast electric field pulses decays exponentially in time with timescale τ. To measure multiple periods of oscillation $2\pi/\bar{\omega} \ll \tau$.

Figure 3 shows the contribution to the current arising from contributions $\boldsymbol{j}_A(\boldsymbol{k}, t)$ for a system with $\boldsymbol{b} = (0.5, 0.2)v_f$, $v_f = 10^6$ m/s, and $\tau = 6.3 \times 10^{-15}$ s perturbed by an electric field pulse with $\Delta_t = 0.2$ ps and $E_0 = 5$ MV/cm. In Fig. 3(a) the system has a small gap size with $m_0 = 0.001\hbar v_f/a$. The intraband contribution to the current as a function of time is plotted for this system at two different chemical potentials, $\mu = -1.2$ meV and $\mu = -2.3$ meV. The currents are shown to modulate in time with mean terahertz frequencies $\bar{\omega} = 2.79 \times 10^{12}$ s^{-1} and $\bar{\omega} = 4.21 \times 10^{12}$ s^{-1}, respectively. In Fig. 3(b) the system has a large gap size $m_0 = 0.5\hbar v_f/a$. Again, the intraband contribution to the current is shown for two different chemical potentials, $\mu = -1.37$ eV and $\mu = 1.81$ eV. The average petahertz frequency modulations of the currents are $\bar{\omega} = 2.86 \times 10^{15}$ s^{-1} and $\bar{\omega} = 3.69 \times 10^{15}$ s^{-1}, respectively. These examples demonstrate the robustness to generate coherent oscillating currents at frequencies from terahertz all the way to petahertz by manipulation of a chemical potential.

In contrast, Fig. 4 shows an example of the contribution to the current arising from contributions $\boldsymbol{j}_B(\boldsymbol{k}, t)$ for a system with $\boldsymbol{b} = (0.5, 0.2)v_f$, $v_f = 10^6$ m/s, $\tau = 6.3 \times 10^{-15}$, $m_0 = 0.5\hbar v_f/a$, and $\mu = -1.37$ eV perturbed by an external field with $\Delta_t = 0.2$ ps and $E_0 = 5$ MV/cm. These contributions tend to add incoherently across the Brillouin zone, leading to a nonoscillatory current that decays exponentially in time.

VI. CONCLUSION

Here we have demonstrated that ultrafast electronic field pulses can induce currents nonlinear in the perturbing electric field that modulate at a frequency determined by the energy differences between bands. These oscillating currents arise from interband transitions from electronic states on the Fermi surface to unoccupied states with equal crystal momentum. Other contributions to the current derive from matrix elements located across the Brillouin zone that oscillate with a wide range of frequencies and ultimately lead to an incoherent superposition of terms that result in nonoscillatory current behavior. The frequency of the intraband contribution to the current can be manipulated by changing the chemical potential which tunes the average energy difference between states on the Fermi surface and states above it. This tool, in principle, can be used as a mechanism for generating currents that oscillate at various frequencies from THz to the near IR.

Once an induced current is generated, it can radiate into the outgoing solutions of the Maxwell wave equation,

$$j_i^{\text{ind}}(\boldsymbol{r}, t) = \sum_j \frac{1}{\mu_0}\left(\delta_{ij}\frac{1}{c^2}\frac{\partial^2}{\partial t^2} - \nabla\cdot\nabla + \partial_{r_i}\partial_{r_j}\right)A_j^{\text{ind}}(\boldsymbol{r}, t). \tag{21}$$

Induced charge currents at frequency ω will generate induced electromagnetic fields $\boldsymbol{A}^{\text{ind}}(\boldsymbol{r}, t)$ at the same frequency.

For high-frequency current modulations, measurement of these induced electromagnetic fields can be done through techniques like attosecond interferometry [29]. Studying the high-frequency electronic dynamics in materials creates a new platform for ultrafast electronic logic and signal processing. Identifying the precise mechanism for their generation now allows for the development of new control and manipulation protocols implemented in the context of semiconductor band engineering.

ACKNOWLEDGMENT

Z.A. and E.J.M. are supported by the Department of Energy under Grant No. DE-FG02-84ER45118.

[1] O. Keller, Theoretical study of the nonlinear response function describing optical second-harmonic generation in nonlocal metal optics, Phys. Rev. B **31**, 5028 (1985).

[2] T. G. Pedersen, Intraband effects in excitonic second-harmonic generation, Phys. Rev. B **92**, 235432 (2015).

[3] T. Morimoto and N. Nagaosa, Topological nature of nonlinear optical effects in solids, Sci. Adv. **2**, e1501524 (2016).

[4] F. de Juan, A. G. Grushin, T. Morimoto, and J. E. Moore, Quantized circular photogalvanic effect in Weyl semimetals, Nat. Commun. **8**, 15995 (2017).

[5] Z. Ji, G. Liu, Z. Addison, W. Liu, P. Yu, H. Gao, Z. Liu, A. M. Rappe, C. L. Kane, E. J. Mele *et al.*, Spatially dispersive circular photogalvanic effect in a Weyl semimetal, Nat. Mater. **18**, 955 (2019).

[6] N. Dudovich, O. Smirnova, J. Levesque, Y. Mairesse, M. Y. Ivanov, D. Villeneuve, and P. B. Corkum, Measuring and controlling the birth of attosecond XUV pulses, Nat. Phys. **2**, 781 (2006).

[7] M. Schultze, E. M. Bothschafter, A. Sommer, S. Holzner, W. Schweinberger, M. Fiess, M. Hofstetter, R. Kienberger, V. Apalkov, V. S. Yakovlev *et al.*, Controlling dielectrics with the electric field of light, Nature (London) **493**, 75 (2013).

[8] F. Krausz and M. I. Stockman, Attosecond metrology: From electron capture to future signal processing, Nat. Photonics **8**, 205 (2014).

[9] M. Lucchini, S. A. Sato, A. Ludwig, J. Herrmann, M. Volkov, L. Kasmi, Y. Shinohara, K. Yabana, L. Gallmann, and U. Keller, Attosecond dynamical Franz-Keldysh effect in polycrystalline diamond, Science **353**, 916 (2016).

[10] H. Mashiko, K. Oguri, T. Yamaguchi, A. Suda, and H. Gotoh, Petahertz optical drive with wide-bandgap semiconductor, Nat. Phys. **12**, 741 (2016).

[11] M. Schultze, K. Ramasesha, C. Pemmaraju, S. Sato, D. Whitmore, A. Gandman, J. S. Prell, L. Borja, D. Prendergast, K. Yabana *et al.*, Attosecond band-gap dynamics in silicon, Science **346**, 1348 (2014).

[12] D. Golde, T. Meier, and S. W. Koch, High harmonics generated in semiconductor nanostructures by the coupled dynamics of optical inter- and intraband excitations, Phys. Rev. B **77**, 075330 (2008).

[13] M. Hohenleutner, F. Langer, O. Schubert, M. Knorr, U. Huttner, S. W. Koch, M. Kira, and R. Huber, Real-time observation of interfering crystal electrons in high-harmonic generation, Nature (London) **523**, 572 (2015).

[14] J. E. Sipe and A. I. Shkrebtii, Second-order optical response in semiconductors, Phys. Rev. B **61**, 5337 (2000).

[15] D. E. Parker, T. Morimoto, J. Orenstein, and J. E. Moore, Diagrammatic approach to nonlinear optical response with application to Weyl semimetals, Phys. Rev. B **99**, 045121 (2019).

[16] D. J. Passos, G. B. Ventura, J. M. Viana Parente Lopes, J. M. B. Lopes dos Santos, and N. M. R. Peres, Nonlinear optical responses of crystalline systems: Results from a velocity gauge analysis, Phys. Rev. B **97**, 235446 (2018).

[17] P. Král, Quantum kinetic theory of shift-current electron pumping in semiconductors, J. Phys.: Condens. Matter **12**, 4851 (2000).

[18] F. Nastos and J. E. Sipe, Optical rectification and shift currents in GaAs and gap response: Below and above the band gap, Phys. Rev. B **74**, 035201 (2006).

[19] M. Bieler, K. Pierz, and U. Siegner, Simultaneous generation of shift and injection currents in (110)-grown GaAs/AlGa as quantum wells, J. Appl. Phys. **100**, 083710 (2006).

[20] S. M. Young and A. M. Rappe, First Principles Calculation of the Shift Current Photovoltaic Effect in Ferroelectrics, Phys. Rev. Lett. **109**, 116601 (2012).

[21] L. Z. Tan, F. Zheng, S. M. Young, F. Wang, S. Liu, and A. M. Rappe, Shift current bulk photovoltaic effect in polar materials-hybrid and oxide perovskites and beyond, npj Comput. Mater. **2**, 1 (2016).

[22] A. M. Cook, B. M. Fregoso, F. de Juan, S. Coh, and J. E. Moore, Design principles for shift current photovoltaics, Nat. Commun. **8**, 14176 (2017).

[23] C. Timm and K. Bennemann, Response theory for time-resolved second-harmonic generation and two-photon photoemission, J. Phys.: Condens. Matter **16**, 661 (2004).

[24] J. von Neumann, Wahrscheinlichkeitstheoretischer aufbau der quantenmechanik, Nachr. Ges. Wiss. Göttingen, Math.-Phys. Kl. **1927**, 245 (1927).

[25] G. B. Ventura, D. J. Passos, J. M. B. Lopes dos Santos, J. M. Viana Parente Lopes, and N. M. R. Peres, Gauge covariances and nonlinear optical responses, Phys. Rev. B **96**, 035431 (2017).

[26] E. I. Blount, Formalisms of band theory, in *Solid State Physics*, edited by F. Seitz and D. Turnbull (Academic Press, New York, 1962), Vol. 13, pp. 305–373.

[27] A. Sekine, D. Culcer, and A. H. MacDonald, Quantum kinetic theory of the chiral anomaly, Phys. Rev. B **96**, 235134 (2017).

[28] P. Földi, Gauge invariance and interpretation of interband and intraband processes in high-order harmonic generation from bulk solids, Phys. Rev. B **96**, 035112 (2017).

[29] H. Mashiko, Y. Chisuga, I. Katayama, K. Oguri, H. Masuda, J. Takeda, and H. Gotoh, Multi-petahertz electron interference in Cr: Al_2O_3 solid-state material, Nat. Commun. **9**, 1 (2018).